



# Variations in the concentration, source and flux of polycyclic aromatic hydrocarbons in sediments of the Pearl River Estuary: Implications for anthropogenic impacts

Yali Li<sup>a,b,1</sup>, Nairong Guo<sup>a,b,1</sup>, Ke Yuan<sup>a,b</sup>, Baowei Chen<sup>a,b</sup>, Junjie Wang<sup>c</sup>, Maofeng Hua<sup>a</sup>, Jing Yu<sup>a</sup>, Jingyan Hu<sup>a</sup>, Run Lu<sup>a</sup>, Shichun Zou<sup>a,b</sup>, Ying Yang<sup>a,b,\*</sup>

<sup>a</sup> School of Marine Sciences, Sun Yat-sen University, and Southern Marine Science and Engineering Guangdong Laboratory (Zhuhai), Zhuhai 519082, China

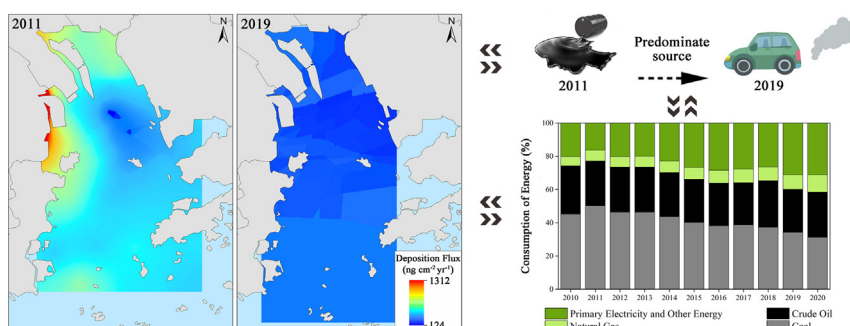
<sup>b</sup> Pearl River Estuary Marine Ecosystem Research Station, Ministry of Education, Zhuhai 519082, China

<sup>c</sup> Department of Earth Sciences – Geochemistry, Faculty of Geosciences, Utrecht University, Princetonlaan 8a, Utrecht 3584CB, the Netherlands

## HIGHLIGHTS

- The PAH concentrations in the PRE have decreased by 50 % from 2011 to 2019.
- The predominant source has changed from petroleum to traffic emission.
- The deposition flux has decreased 203.39 ng cm<sup>-2</sup> yr<sup>-1</sup> in nearly decade.
- The PAH changes in PRE sediment reflect the local energy structure transformation.

## GRAPHICAL ABSTRACT



## ARTICLE INFO

Editor: Paromita Chakraborty

### Keywords:

PAHs  
Sediments  
Mass inventory  
Deposition flux  
Source composition  
Pearl River Estuary

## ABSTRACT

Variations in the distribution, source composition, mass inventory and burial flux of polycyclic aromatic hydrocarbons (PAHs) in surface sediments from the Pearl River Estuary (PRE) collected in 2011 and 2019 were analyzed to investigate the influence of the anthropogenic activities. Total concentrations of 16 priority PAHs in 2019 ( $200.40 \pm 188.86$  ng g<sup>-1</sup> dry weight on average) were at the medium level among global bays/estuaries/coastal areas. In 2019, PAH concentrations have decreased by about 50% compared to 2011 and the dominant composition has changed from low- to high-molecular-weight PAHs. The qualitative and quantitative source apportionment analysis indicates that the dominant source of PAHs has shifted from petroleum (40.33%) in 2011 to traffic emission (44.17%) in 2019. The source variation in the PRE can be attributed to the transformation of the energy source structure from petrogenic to pyrogenic in the Pearl River Delta. The estimated PAH mass inventory of the top 5-cm sediment was 38.70 metric tons in 2019, which was about 41 metric tons lower than that in 2011. The average deposition fluxes have dropped from  $418.91 \pm 261.02$  ng cm<sup>-2</sup> yr<sup>-1</sup> in 2011 to  $215.52 \pm 246.63$  ng cm<sup>-2</sup> yr<sup>-1</sup> in 2019. The decreasing PAH concentration is related to the sediment coarsening and decline of total organic carbon. These findings in the PRE can be applied to other estuarine environments influenced by anthropogenic activities.

\* Corresponding author at: School of Marine Sciences, Sun Yat-sen University, Southern Marine Science and Engineering Guangdong Laboratory (Zhuhai), Zhuhai 519082, China.  
E-mail address: [yingyang6@mail.sysu.edu.cn](mailto:yingyang6@mail.sysu.edu.cn) (Y. Yang).

<sup>1</sup> These authors contributed equally to this work.

## 1. Introduction

Estuaries are sensitive to anthropogenic impacts (Bouloubassi et al., 2012). On one hand, estuaries are important channels through which terrigenous materials are transported to the ocean (Nedwell et al., 1999; Zhang et al., 2019). The large amounts of terrigenous nutrient inputs support high biological productivity and biodiversity in estuarine areas, which make them key system in global biogeochemical cycle; on the other hand, estuarine environments are increasingly exposed to large amounts of anthropogenic chemical pollutants and become an important sink of chemical pollutants, e.g. heavy metals, excessive nutrients and persistent organic pollutants (POPs) (Wang et al., 2017; Zhu et al., 2021). Pollution in estuaries has become an increasing global concern for environmental conservation and ecological restoration.

Polycyclic aromatic hydrocarbons (PAHs) are the major organic contaminants in the estuarine environment (Pintado-Herrera et al., 2017). More than 200 PAHs are ubiquitous in various environments and 16 of them are listed as pollutants under priority control by the United States Environmental Protection Agency (USEPA) due to their high toxicity, carcinogenicity, mutagenicity and bioaccumulation property (USEPA, 1992). PAHs are mainly derived from anthropogenic sources such as incomplete combustion of biological organic matter and fossil fuel, traffic emission and ship spill (Neff, 1979; Wang et al., 2017; Li et al., 2021a). As a result of the intensified human activities, PAHs emissions are significantly higher at present than in the preindustrial era (Vila-Costa et al., 2020). Anthropogenic PAHs enter the estuaries and coastal regions mainly via river input and atmospheric deposition and can easily bind to sediments due to their hydrophobicity. PAH deposition fate in estuaries could be impacted by sedimentary properties such as grain size, total organic carbon (TOC) and deposition rate (Wang et al., 2017; Huang et al., 2021a, 2021b). Therefore, PAHs distributions pattern and their burial fate in estuarine sediments could not only indicate the change in sedimentary environment, but also be regarded as a good indication of anthropogenic impacts (Kanwischer et al., 2020).

The Pearl River Estuary (PRE) links the vast Pearl River network and the South China Sea with several outlets and receives material inputs from multiple sources (Hu et al., 2011). The urbanization and industrialization of the Pearl River Delta (PRD) have been remarkably accelerated since the implementation of China's Reform and Opening-up in 1978 (Feng and Fan, 2018; Yang et al., 2019), with significant increase in associated environment pollution reported in the PRE (Yuan et al., 2015; Pintado-Herrera et al., 2017). PAHs emitted from the PRD could enter the PRE and exert long-term adverse effects on estuarine ecosystem (Chen et al., 2006; Yuan et al., 2015). The PAHs mass inventories of the surface sediment of 2012 were estimated to be about 50 tons (Pintado-Herrera et al., 2017) and the contaminated sediments of the PRE were regarded as an important "sink" of PAHs (Chen et al., 2006). In addition, the all-year-round high temperature in the subtropical PRE may enhance the global fractionation effect of volatile organic pollutants (Chen et al., 2006) and thus the sediment may potentially shift from a "sink" to "source" of PAHs to the global atmosphere. In the past decades, PAH concentrations, sources and ecological risk of marine sediments have been extensively investigated in the PRE (Chen et al., 2006; Yuan et al., 2015; Pintado-Herrera et al., 2017; Li et al., 2021b). However, most of them focused on the current pollution status and lack trend analysis based on time series. Moreover, the rapid economic development of Guangdong-Hong Kong-Macao Greater Bay Area (GBA) will inevitably change the distribution, source and burial fate of PAHs and further threaten the ecological safety in the PRE.

Therefore, the main goals of this study were to (1) present a comprehensive, observation-based study on the concentrations, composition, spatial distribution and temporal changes of PAHs in sediments of the PRE, (2) quantify the contributions of different PAH sources and their nearly-decadal changes in response to anthropogenic activities, (3) analyze the mass inventory and deposition flux of PAHs in sediments, and (4) explore the influence of human perturbations on PAHs fate in the PRE.

## 2. Materials and methods

### 2.1. Study area

The Pearl River is the second largest river in China in terms of discharge and carries large amounts of suspended particles ( $8.72 \times 10^7 \text{ t yr}^{-1}$ ). These sediments enter the South China Sea from the Pearl River through 8 major outlets (Zhu et al., 2021, Fig. 1). The PRE is the largest estuary of the Pearl River, which receives 56.8% of the riverine sediment load through 4 eastern outlets i.e., Humen, Jiaomen, Hongqimen and Hengmen (Zhang and Huang, 2005). The funnel-shaped PRE is topographically characterized by 2 channels (the West and East Channels, with depths of >10 m and 5–15 m, respectively) and 3 shoals (the West, Middle and East Shoals, all with depths <5 m, Fig. 1, Zhang et al., 2019).

### 2.2. Sample collection and analysis

A total of 26 surface sediment samples (0–5 cm depth) were collected from the PRE in both August 2011 and September 2019 using stainless steel grab (Fig. S1 and Fig. 1). The sampling of sediment was described in more detail in Yuan et al. (2015). All sediments were sealed in plastic bags immediately and stored in freezer at  $-20^\circ\text{C}$  until further treatment. Sediment samples were firstly homogenized and freeze-dried. PAHs in sediment were extracted with the Soxhlet extraction method. The extracted liquid was first purified by a chromatographic column, then condensed with rotary evaporator and further concentrated to 1 mL with a gentle nitrogen flow. Detailed procedure for sediment pre-treatment can be found in Yuan et al. (2015) and Li et al. (2021b).

In order to measure the grain size, portions of the sediments were pretreated with  $\text{H}_2\text{O}_2$  solution (20%) and 15% HCl solution to scavenge organic matter. The grain size of the samples was measured with a laser diffraction particle size analyzer (LS13,320). Sediment samples for TOC content detection were decalcified with 1 M HCl and dried at  $60^\circ\text{C}$ . TOC content was measured with an elemental analyzer (Vario ISOPOTE Cube-Isoprime, Elementar). More information about the method can be found in Huang et al. (2021a, 2021b) and Lin and Lin. (2022).

Total concentrations of 16 priority PAHs in the sediments were measured with Agilent 5977B GC/MSD (7890B GC system) using a quartz capillary HP-5MS column ( $30 \text{ m} \times 0.25 \text{ mm} \times 0.25 \mu\text{m}$  film thickness, Agilent). The 16 priority PAHs are naphthalene (Nap), acenaphthylene (Acy), acenaphthene (Ace), fluorene (Flu), phenanthrene (Phe), anthracene (Ant), fluoranthene (Flo), pyrene (Pyr), benzo[a]anthracene (BaA), chrysene (Chr), benzo[b]fluoranthene (BbF), benzo[k]fluoranthene (BkF), benzo[a]pyrene (BaP), dibenzo[ah]anthracene (DahA), benzo[ghi]perylene (BghiP), and Indeno[123-cd]pyrene (IcdP) (USEPA, 1992). Selected ion reaction monitoring (SIM) mode was applied for quantitative analyses.

### 2.3. Quality assurance/quality control (QA/QC)

A procedural blank and duplicate sample were analyzed every 12 samples. No PAHs were detected in procedural blanks. The concentration difference between duplicate samples was <15%. External standard method (Wang et al., 2015) was used for the quantitative analysis of every single PAH compound with a six-point calibration curve applied. The average recovery of surrogate standards varied from 42.0% (for Naphthalene- $\text{d}_8$ ) to 106.5% (for Perylene- $\text{d}_{12}$ ).

### 2.4. Data analysis

#### 2.4.1. Source apportionment analysis of PAHs

Molecular diagnostic ratio (MDR) method and US-EPA positive matrix factorization (PMF) model (version 5.0) (Yunker et al., 2002) were used for source apportionment of PAHs in sediments.

- MDR: qualitative analysis

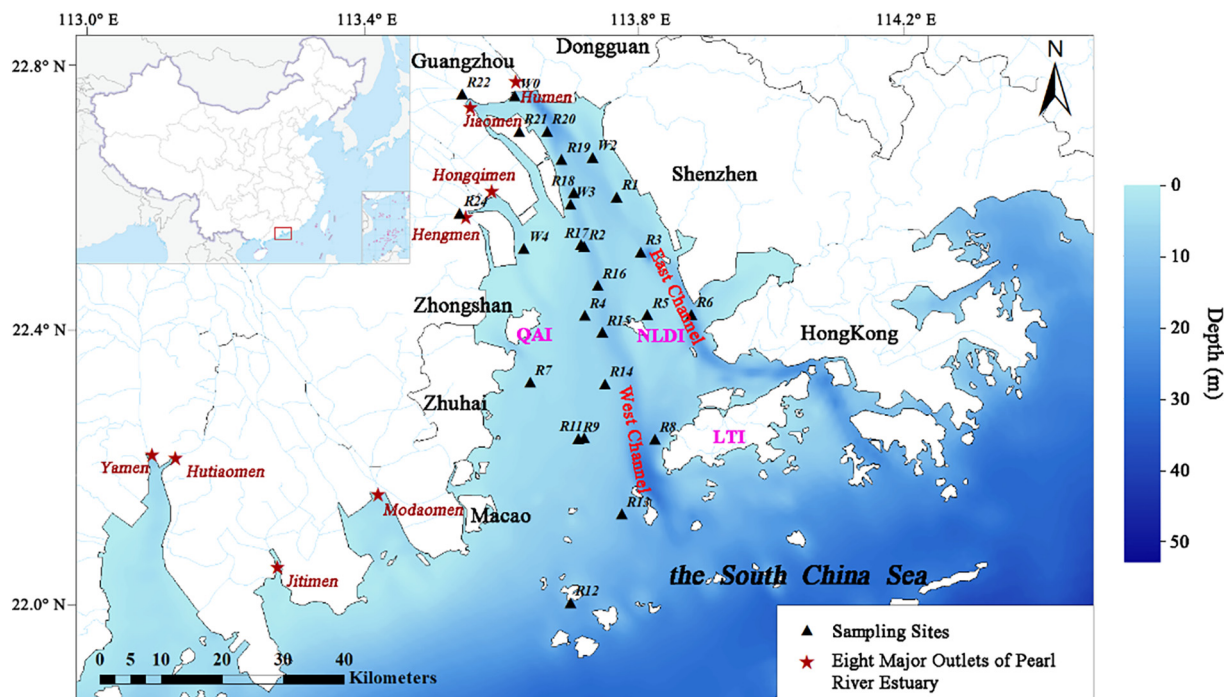


Fig. 1. Sample location in the Pearl River Estuary in 2019 (QAI: Qi'ao Island; NLDI: Neilingding Island; LTI: Lantau Island).

Since PAHs generated from different sources have different component spectra, the types of pollution sources can therefore be distinguished based on their corresponding characteristic ratios (Yunker et al., 2002). Molecular ratios of Flo/(Flo + Pyr) and BaA/(BaA + Chr) are often used for the PAHs source analysis. Flo/(Flo + Pyr) ratio of <0.4, 0.4–0.5 and >0.5 indicate source of petroleum, petroleum and combustion mixed, and combustion, respectively; BaA/(BaA + Chr) ratios of <0.2, 0.2–0.35 and >0.35 indicate sources of petroleum, petroleum and combustion mixed, and combustion, respectively.

#### • PMF: quantitative analysis

The analytical PMF model includes 1) preparing concentration data and uncertainty files, 2) running the PMF5.0 program, and 3) parsing the major sources when the ratio of theoretical Q value (Q is the objective function of the PMF model, i.e., the sum of all sample residuals and their uncertainties) to robust Q value is in a reasonable range of 0–1.5 (Maria et al., 2018).

The equation of the PMF model can be expressed as:

$$X_{ij} = \sum_{k=1}^p G_{ik} F_{kj} + e_{ij} (i = 1, 2, \dots, n; j = 1, 2, \dots, m; k = 1, \dots, p) \quad (1)$$

where  $X_{ij}$  is the contribution matrix of sample  $i \times$  chemical component  $j$ ,  $F_{kj}$  is the source profile matrix of pollution source  $k \times j$ ,  $G_{ik}$  is the contribution rate matrix of  $i \times k$ ,  $n$  is the number of samples,  $m$  is the number of chemical components,  $p$  is the number of major pollution sources, and  $e_{ij}$  is the residual matrix of  $i \times j$ .

The PMF model combines the sum of all sample residuals and their uncertainties as an objective function Q:

$$Q = \sum_{i=1}^n \sum_{j=1}^m \left( \frac{e_{ij}}{\varepsilon_{ij}} \right)^2 \quad (2)$$

where  $\varepsilon_{ij}$  is the uncertainty of  $j$  in sample  $i$ . The constraint conditions of the PMF model are that  $G$  and  $F$  are non-negative matrices. In this study, a robust model was adopted to eliminate the influence of extreme values (i.e., outliers) (Paatero and Tapper, 1994).

As for PAH source identification, previous studies indicate that Flo, Acy, and Pyr indicate a source of coal combustion (Yunker et al., 2002), Chr and BaA can be linked to a source of natural gas combustion (Lin et al., 2017), the HMW PAHs (including BaA, BkF, BaP, IcdP, DahA, and BghiP) mainly originate from incomplete combustion of fossil fuels, BkF, BaP, BghiP, and IcdP are the products of automobile exhaust emissions (Yang et al., 2013), BkF and IcdP are related to diesel combustion, and BghiP is related to gasoline combustion (Ribeiro et al., 2012; Han et al., 2021).

The PAH spatial distribution, deposition rate, grain size and TOC content were obtained by the Kriging interpolation method by ArcGIS 10.7. SPSS 26 was used for the Pearson correlation analysis between the PAH concentration and grain size or TOC content in the sediments.

#### 2.4.2. Mass inventory and deposition flux

##### • Mass inventory

To estimate the accumulation of PAHs in the surface sediments of the PRE, the mass inventories ( $I$ ) of PAHs were calculated as:

$$I = \sum k C_i A_i d \rho \quad (3)$$

where  $k$  is the conversion factor,  $C_i$  is the average concentration of  $\Sigma_{16}$  PAHs in  $i$ th region ( $\text{ng g}^{-1}$ ),  $A_i$  is the area of each sub-region ( $\text{in km}^2$ ),  $d$  is the thickness of the sediment ( $\text{in cm}$ ),  $\rho$  is the density of the dry sediment particles ( $\text{in g cm}^{-3}$ , Chen et al., 2006). The sediment thickness was 5 cm. A recommended value of  $1.5 \text{ g cm}^{-3}$  was selected for  $\rho$  as suggested by Pintado-Herrera et al., (2017).

##### • Deposition flux

To assess the potential threat and the extent of contamination of PAHs in sediments of the PRE, the PAHs deposition flux was calculated as (Fang et al., 2015):

$$\text{PAH deposition flux} = C_i \times \rho \times \omega \times (1 - \phi) \quad (4)$$



where  $C_i$  is the average concentration of  $\Sigma_{16}$  PAHs in region  $i$  ( $\text{ng g}^{-1}$ ),  $\rho$  is the density of the dry sediment particles ( $1.5 \text{ g cm}^{-3}$ ),  $\omega$  is the sedimentation rate of each sub-region ( $\text{cm yr}^{-1}$ , Fig. 4) and  $\phi$  is the sediment porosity which is widely used as a constant of 0.672 (Wang et al., 2016). Grain size data ( $n = 106$ ) were mainly from Zhang et al., (2013), and the overall datasets of deposition rates ( $n = 35$ ) were listed in Tables S3 and S4.

### 3. Results and discussion

#### 3.1. Distribution patterns of PAHs in the PRE

##### 3.1.1. Spatial and temporal variations of PAHs in 2011 and 2019

Generally, the total concentration of the 16 PAHs ( $\Sigma_{16}$  PAHs) varied considerably among samples from 2019 (Table S1), ranging from 20.44 to 678.66  $\text{ng g}^{-1}$  in dry weight (dw), with an average value of  $200.40 \pm 188.86 \text{ ng g}^{-1}$  dw (Fig. 2b). The distribution of  $\Sigma_{16}$  PAHs in the PRE was heterogeneous, with the highest concentration observed at the West Channel between the Qi'ao Island (QAI) and Neilingding Island (NLDI). Other hotspots with high  $\Sigma_{16}$  PAHs concentrations were at the Humen Outlet and near the coast of Shenzhen. This is probably because around 75.5% of the discharge at the Humen outlet is from the East and North Rivers, which flow across the most prosperous and densely populated areas and receives large amounts of associated pollutant inputs (Yuan et al., 2015). After exiting the Humen Outlet, most sediments and adsorbed organic pollutants were deposited when flowing through the West Channel due to the jacking effect of tidal currents. The concentration of  $\Sigma_{16}$  PAHs was also high near the Shenzhen Bao'an International Airport (Fig. 2b), which can be explained by the exhaust from aircraft fuel and pollutants from nearby petrochemical plants via atmospheric deposition and riverine export.

The average concentration of  $\Sigma_{16}$  PAHs in 2011 was  $437.46 \pm 196.82 \text{ ng g}^{-1}$  dw ( $159.80\text{--}897.49 \text{ ng g}^{-1}$  dw), which was higher than that in 2019 (Fig. 2a, b). In 2011, the highest concentration (of  $897.49 \text{ ng g}^{-1}$ ) was observed at the head of the estuary near Humen Outlet, followed by another hotspot near the southeast of Macao in the southern part of the PRE (Fig. 2a). In general, the heavy-PAH-pollution region in the PRE moved from the northern and southern parts in 2011 to the middle region in 2019. Moreover,  $\Sigma_{16}$  PAHs have been decreasing. This trend was generally consistent with the PAHs record in sediment core in the South China Sea (Liu et al., 2012).

The 16 priority PAHs were categorized into two groups of the low-molecular-weight (LMW, i.e., PAHs with 2–3 aromatic rings) and high-molecular-weight (HMW, i.e., PAHs with 4–6 aromatic rings) PAH compounds to explore the changes of PAHs in 2011 and 2019 (Fig. 2c–f). In 2011, the concentrations of LMW and HMW PAHs were both low in the middle estuary. High concentrations of LMW PAHs were observed in the area close to Macao while high concentrations of HMW PAHs were found near Dongguan city (Fig. 2c, e). In 2019, high concentrations of LMW and HMW PAHs were both observed in the middle and southern parts of the estuary and high concentrations of HMW PAHs were found also at Humen Outlet and Shenzhen Bao'an International Airport (Fig. 2d, f). The changes in PAH concentrations, composition and their spatial distributions in 2011 and 2019 indicate that the contamination level and emission source have significantly changed during the past years.

The compositions of PAH compounds in the PRE were further compared for 2011 and 2019 in terms of the number of aromatic rings (Fig. 2g–h, S2). In 2011, 4-ring PAHs dominated all sediment samples with an average fraction of 31.71%, followed by 2-ring (31.66%), 3-ring (21.75%), 5-ring (8.83%), and 6-ring PAHs (6.05%). In 2019, 4-ring PAHs remained dominant with a higher average fraction of 45.90%, followed by 3-ring (19.50%), 5-ring (15.68%), 6-ring (11.25%), and 2-ring PAHs (7.67%). Compared to 2011, the fraction of 2-ring PAHs sharply decreased from the 2nd highest to the lowest and that of 3-ring PAHs slightly decreased while 4-ring, 5-ring and 6-ring PAHs largely increased. To sum up, the dominant component in the PAHs shifted from LMW to HMW PAHs in the PRE during the past years.

##### 3.1.2. Pollution level of PAHs in estuaries, bays and coastal areas worldwide

Compared with the reported PAH concentrations in some representative estuaries, bays and coastal areas (Table 1), and PAH concentrations in this study were at the medium level.

The average concentrations of  $\Sigma_{16}$  PAHs in the estuaries of large rivers of China such as Pearl River, Yangtze River and Yellow River (i.e., the Bohai Sea mentioned above) are similar (Table 1). The concentrations of  $\Sigma_{16}$  PAHs in the estuaries of large rivers were higher than in the continental shelf regions of marginal seas, polar regions and marine conservation areas, probably because these regions are distant/protected from either river outlets or intense anthropogenic impacts.  $\Sigma_{16}$  PAHs in the estuaries of large rivers are also found to be lower than in coastal wetlands and river deltas, which can be attributed to the PAH absorption and accumulation (largely transported from inland emission sources or contaminated rivers at shorter distances) by abundant organic matter and fine sediment in wetlands (Aiken et al., 2011). However, concentrations of 16 target PAHs were also higher around Nan'ao Island and Ulsan Bay. Nan'ao Island is one of the largest mariculture bases in South China adjacent to fishing harbors and the shipping activities have emitted large amounts of the local PAHs (Gu et al., 2013). As for Ulsan Bay, there is an industrial complex nearby together with an industrial port (Ulsan Port) and thus receives various terrestrial pollutants associated with industrial activities and wastewater discharge (An et al., 2020). Overall, the concentrations of  $\Sigma_{16}$  PAHs in global bays, estuaries and coastal areas seemed to follow the order of the polar regions/marine conservation areas < continental shelf regions of marginal seas < estuaries of large rivers < inland deltas/coastal wetlands, which indicates that the distance from intense anthropogenic impacts may be a crucial factor for PAH pollution status.

#### 3.2. PAH sources and their response to anthropogenic activities

##### 3.2.1. Source apportionment using the qualitative MDR method

Variation of chemical residues in marine sediments can be used as evidence of environmental changes caused by anthropogenic activities (Wang et al., 2022). Different composition of PAHs is proven to be the indicator for different origins of PAHs, with LMW PAHs as indicators for petrogenic origins and HMW PAHs for pyrogenic origins (Yunker et al., 2002). In 2011, 53.41% of the PAHs in the PRE sediment were LMW PAHs, indicating that most of the PAHs were petrogenic. However, in 2019, HMW PAHs (72.81%) became dominant, which indicates that the sources of the PAHs in the PRE have changed from petrogenic to pyrogenic.

The molecular ratios of Flo/(Flo + Pyr) and BaA/(BaA + Chr) from all the PRE sediment samples in 2011 and 2019 were analyzed using the MDR method to qualitatively explore the PAH sources (Fig. 3). In 2011, the ratios were mainly within the ranges of petroleum and the mixed source of petroleum and combustion. Specifically, all the sample ratios of Flo/(Flo + Pyr) in 2011 were lower than 0.4, suggesting the source of petroleum; for the ratios of BaA/(BaA + Chr), 67.86% of the samples were within the range of 0.2–0.35 and 32.14% were lower than 0.2, which indicates the mixed source of petroleum and combustion. In 2019, the ratios of BaA/(BaA + Chr) in the PRE ranged from 0.24 to 0.48 and those of 59.3% of all samples were within the range of 0.2–0.35, indicating a mixed source of petroleum and combustion. The ratios of Flo/(Flo + Pyr) ranged from 0.37 to 0.62, of which 40.74% were between 0.4 and 0.5, indicating a mixed source, and 55.56% of the samples with ratios between 0.5 and 0.6 indicated a combustion source.

Compared to 2011, both ratios of Flo/(Flo + Pyr) and BaA/(BaA + Chr) increased in 2019, which suggested that the dominant source of PAHs in the PRE sediment have shifted from petrogenic (petroleum) to pyrogenic (mixed source of petroleum and combustion).

##### 3.2.2. Quantitative source apportionment using the PMF method

The sedimentary PAH source changed from 3 types for 2011 to 4 types for 2019 (Table 2). Factor 1-2011 and Factor 4-2019 were both dominated by HMW PAHs including BaA, BkF, BaP, BghiP, and IcdP, indicating sources of coal combustion and traffic emission (Yunker et al., 2002;

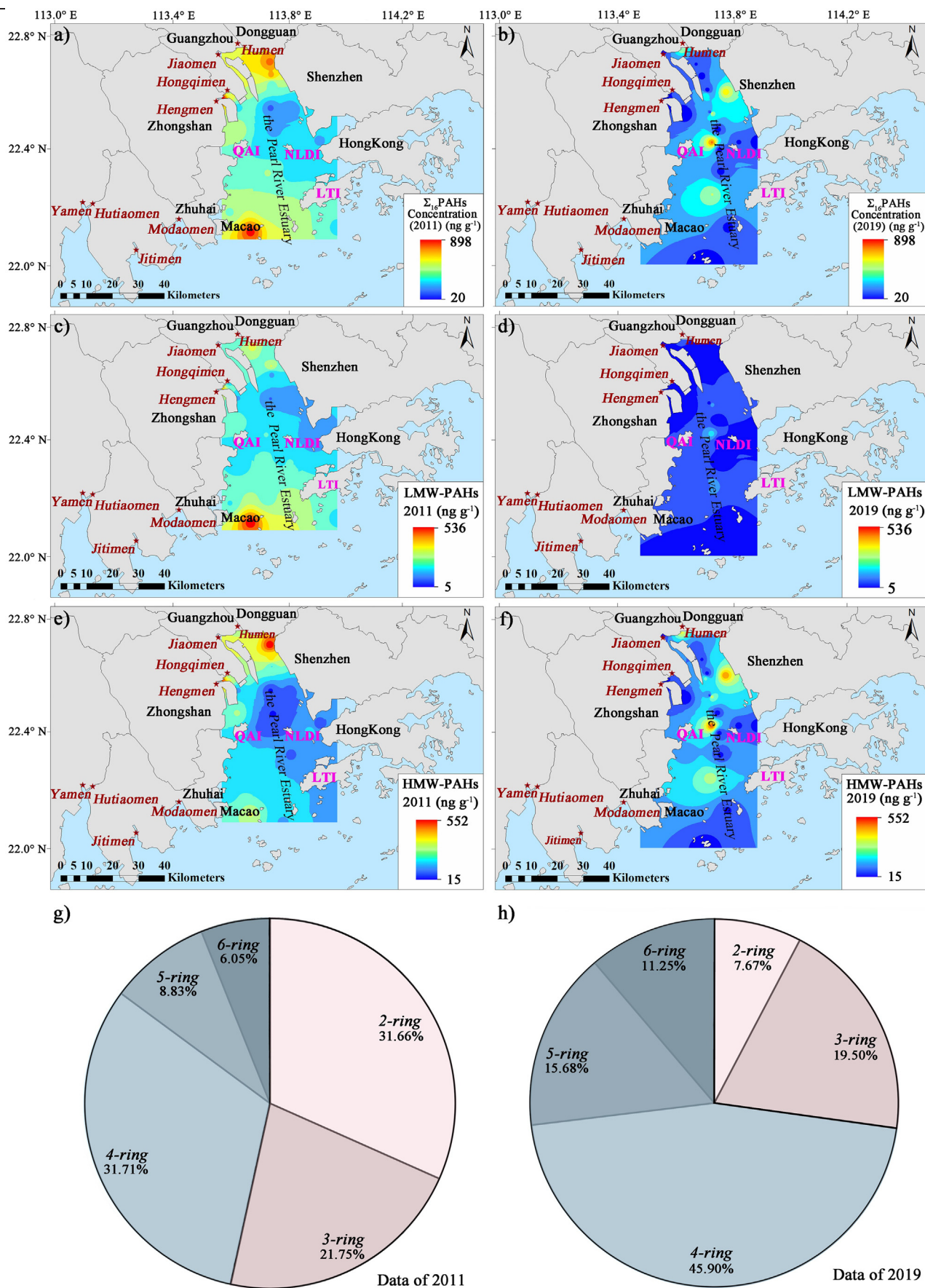


Fig. 2. Spatial distribution of the total concentrations of 16 priority PAHs ( $\Sigma_{16}$  PAHs, a, b), low-molecular-weight (LMW, c, d) and high-molecular-weight (HMW, e, f) PAHs in the Pearl River Estuary and the composition pattern in terms of the number of aromatic rings in the PAH compounds (g, h) in 2011 and 2019.

**Table 1**

PAH concentrations in sediment from the Pearl River Estuary and other estuaries/bays/coastal areas worldwide.

Study area	Sampling time	Number of sampling sites	Number of PAH compounds measured	Concentration range (mean $\pm$ std) (ng g <sup>-1</sup> dw)	Reference
Pearl River Estuary, China	2019	26	16	20.44–678.66 (200.40 $\pm$ 188.86)	This study
Pearl River Estuary, China	2011	26	16	159.80–897.49 (437.46 $\pm$ 196.82)	Yuan et al., 2015
Yazhou Bay of Sanya, China	2020	15	16	13.20–40.37 (31.53)	Han et al., 2021
Northern South China Sea, China	2013–2014	16	15	11.30–95.50 (39.70)	Cai et al., 2017
Western Arctic Ocean	2010	43	16	36.95–150.21 (70.61)	Zhao et al., 2016
Argentine Sea, Northern Patagonian Shelf (marine conservation area)	2015–2016	27	16	19.47–183.92 (82.92)	Oliva et al., 2020
Hainan Island, China	2017	3	16	67.29–196.99 (119.60)	Xiang et al., 2018
East China Sea continental shelf, China	2013–2015	53	16	24.73–420.85 (151.68)	Zhang et al., 2020
Yangtze River Estuary	2017	29	16	57.5–364.5 (166.20)	Zhao et al., 2020
Bohai Sea, China	2016	11	18	25.00–308.00 (184.00)	Wang et al., 2020
Yangtze River Estuary	2010	29	16	90.14–502.12 (221.18)	Li et al., 2012
Nan'ao Island, China	2011	16	16	265.49–951.27 (515.90)	Gu et al., 2013
Yangtze River Delta (near chemical industry parks)	2019	32	19	15.14–5355 (921.00)	Jia et al., 2021
Ulsan Bay, South Korea	2017	9	16	35–4000 (1200.00)	An et al., 2020
Qinhuangdao coastal wetland, China	2016	23	16	341.61–4703.80 (1367.80)	Lin et al., 2018
Coastal site near Bhavnagar, India	2013–2014	24	16	5020–981,180 (34500)	Dudhagara et al., 2016
Matsushima Bay coastal area, Japan	2013	13	16	84–15,548 (–)	Onozato et al., 2020

Yang et al., 2013). Factor 2-2011 and Factor 2-2019 were heavily weighted by Nap, representing a source of petroleum pollution like oil spill (Lemieux et al., 2004). Factor 3-2011 and Factor 1-2019 were dominated by Flu and Phe, which indicated a source of biomass combustion (Ribeiro et al., 2012). Factor 3-2019 accounted for 15.16% and was mainly weighted by BbF indicating a source of petroleum fuel combustion (Duan et al., 2015).

Moreover, quantitative results of the PMF model suggested that respective contribution of the PAHs source has changed prominently from 2011 to 2019. The contribution of the traffic emission, biomass combustion, petroleum spill was 34.52%, 25.15% and 40.33%, respectively in 2011, while it changed to 44.17%, 28.94% and 11.73%, respectively in 2019. The contribution of the traffic emission increased from 34.52% to 44.17%, and the petroleum source decreased from 40.33% to 11.73% from 2011 to 2019. The results of the PMF method indicated that the dominant sedimentary PAHs source in the PRE changed from petroleum to traffic emission.

### 3.3. Mass inventories and deposition fluxes of PAHs in the PRE

PAHs are easily adsorbed on the sediment due to the hydrophobicity of PAH molecules, which makes sedimentary environment an essential factor for PAH distribution and storage in estuarine environment (Strong et al.,

2012; Zhu et al., 2020; Hao et al., 2021). The sediment deposition rate of the PRE presents a significant spatial difference. The West Shoal presented higher deposition rate of the whole PRE, which is much higher than the East Shoal. In addition, deposition rate in inner Lingdingyang region is higher than outer Lingdingyang region. According to the difference of the deposition rates, the PRE was divided into 4 subregions (S1, S2, S3, S4) (Fig. 4), and the average deposition rates were 2.98, 1.58, 1.33 and 1.74 cm yr<sup>-1</sup> respectively.

#### 3.3.1. Mass inventories of PAHs in the PRE

To assess the potential risk of sediments as a contamination source to the estuarine environment, the mass inventories of  $\Sigma_{16}$  PAHs were estimated using a modified approach proposed by Chen et al. (2006). The mass inventories of  $\Sigma_{16}$  PAHs were 79.70 and 38.70 metric tons in 2011 and 2019, respectively (Table S5). According to a previous record, the deposition rate of the PRE ranged from 1.17 cm yr<sup>-1</sup> to 3.01 cm yr<sup>-1</sup>, therefore the mass inventories represented deposits in the past 2 to 4 years.

The inventories of 16 PAHs in 2019 appeared to be 2 times lower than that in 2011. A previous study showed that mass inventory of 16 PAHs in the PRE was 50 metric tons in 2012 (Pintado-Herrera et al., 2017).

**Table 2**

Contribution of various factors (i.e., sources) to different PAH compounds and the total PAHs for 2011 and 2019.

PAH compounds (%)	Main factors-2011			Main factors-2019			
	Factor 1	Factor 2	Factor 3	Factor 1	Factor 2	Factor 3	Factor 4
Nap	19.41	<b>80.59</b>	0.00	29.13	<b>66.71</b>	4.16	0.00
Acy	0.00	50.91	49.09	48.35	5.40	6.10	40.15
Ace	26.59	30.76	42.65	27.82	7.65	26.16	38.36
Flu	7.45	35.32	<b>57.23</b>	<b>65.33</b>	4.28	11.42	18.97
Phe	17.53	30.89	<b>51.57</b>	<b>62.38</b>	4.77	15.04	17.80
Ant	19.6	30.74	49.66	35.23	6.96	9.02	48.79
Flo	45.81	26.8	27.38	43.10	8.53	13.8	34.58
Pyr	43.01	23.43	33.56	30.04	3.06	13.86	<b>53.03</b>
BaA	<b>74.72</b>	0.00	25.28	17.32	5.79	16.79	<b>60.10</b>
Chr	<b>57.12</b>	19.95	22.93	32.23	6.68	17.21	43.88
BbF	<b>63.21</b>	15.01	21.78	32.78	0.00	<b>66.62</b>	0.60
BkF	<b>62.91</b>	14.02	23.08	23.25	9.24	0.00	<b>67.51</b>
BaP	<b>59.82</b>	13.12	27.05	10.63	10.00	9.61	<b>69.76</b>
IcdP	<b>59.19</b>	31.13	9.67	3.35	9.74	17.87	<b>69.04</b>
DahA	<b>62.64</b>	15.31	22.05	0.00	9.61	45.45	44.94
BghiP	<b>75.27</b>	9.55	15.18	2.09	6.95	9.69	<b>81.27</b>
Total PAHs	34.52	40.33	25.15	28.94	11.73	15.16	44.17

Notes: Values &gt; 50 are Highlighted.

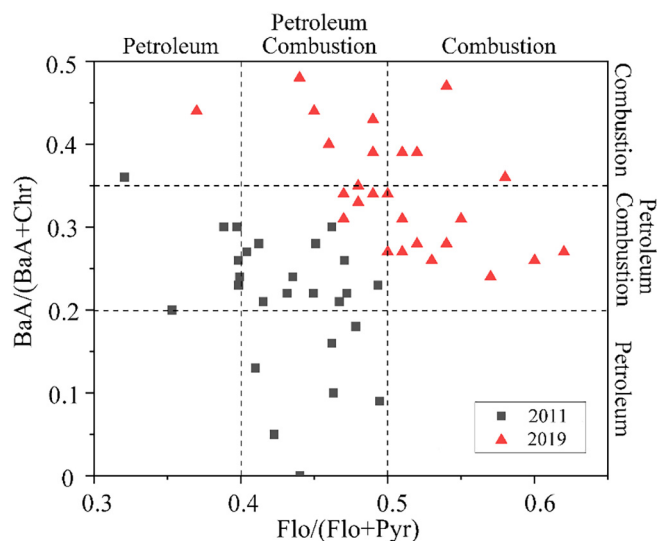


**Fig. 3.** Molecular ratios of BaA/(BaA + Chr) vs. Flo/(Flo + Pyr) in sediment in the Pearl River Estuary in 2011 and 2019.



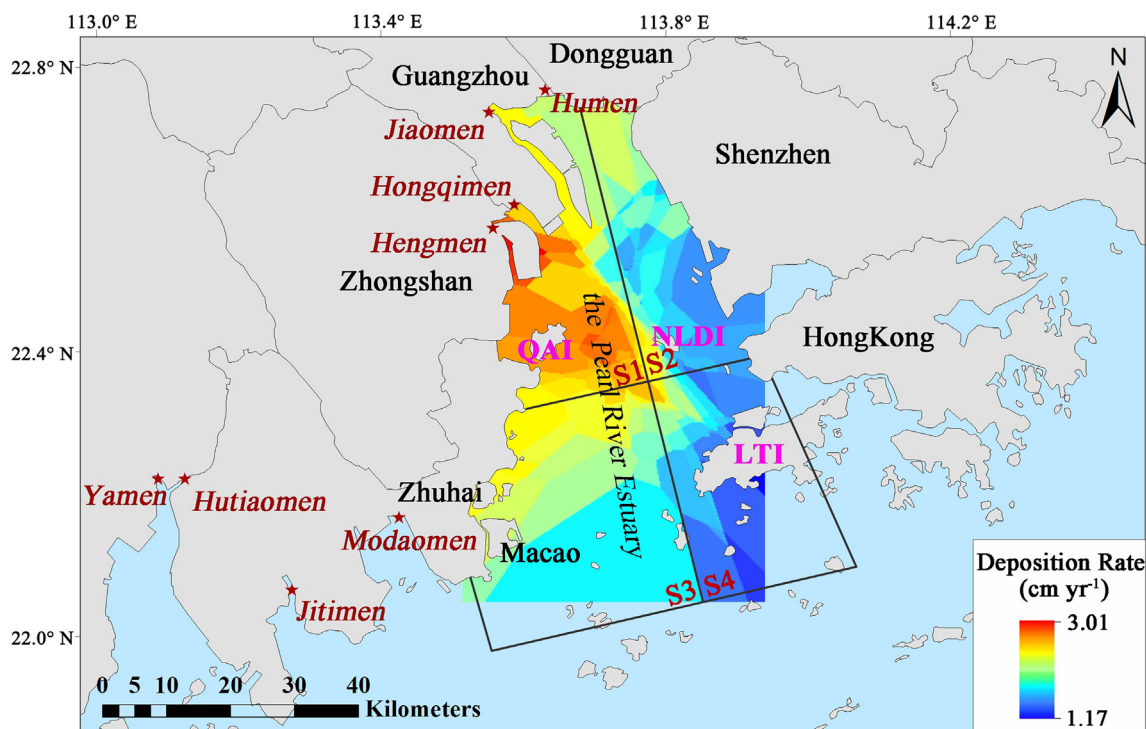


Fig. 4. The distribution of the deposition rate in the Pearl River Estuary (reanalysis from reported data in Table S3 and S4).

Considering the results in this study, the mass inventory of PAHs in the PRE has decreased during 2012–2019.

### 3.3.2. Deposition flux of PAHs in the PRE

As an important sink of PAHs, deposition flux of PAHs in estuary and continental shelf have raised more and more concerns (Qin et al., 2011; Lin et al., 2013; Wang et al., 2017). Deposition flux was more widely used as an indication of the contamination capacity of marine sediment because it was not affected by input sources and the dilution effect of the terrigenous pollutants (Fang et al., 2015; Wang et al., 2020).

In 2011, the PAH deposition fluxes in the PRE ranged from 124.58 to 1316.67  $\text{ng cm}^{-2} \text{yr}^{-1}$ , with an average of  $418.91 \pm 261.02 \text{ ng cm}^{-2} \text{yr}^{-1}$ . In 2019, the PAH deposition fluxes in the PRE ranged from 25.90 to 995.63  $\text{ng cm}^{-2} \text{yr}^{-1}$ , and averaged  $215.52 \pm 246.63 \text{ ng cm}^{-2} \text{yr}^{-1}$ . Overall, the PAHs burial capacity has been decreasing and presented large spatial differentiation (Fig. 5). In 2011, the highest PAH deposition flux was located near the outlets (Hongqimen, 1316.67  $\text{ng cm}^{-2} \text{yr}^{-1}$ ;

Humen, 770  $\text{ng cm}^{-2} \text{yr}^{-1}$ ) and the West Shoal (P20, 722.65  $\text{ng cm}^{-2} \text{yr}^{-1}$ ), and the West Shoal exhibited higher PAHs fluxes than the East Shoal (Fig. 5a). In 2019, the highest PAHs flux was observed in the middle of the PRE (995.63  $\text{ng cm}^{-2} \text{yr}^{-1}$ ), and the average value of PAHs flux for East Shoal was higher than West Shoal (Fig. 5b).

According to the variation of deposition rate, the PRE was divided into 4 subregions to calculate the respective PAH sink flux (Table S5). The 4 subregions were the West Shoal (S1), the East Shoal (S2), the west section of the outer Lingdingyang (S3) and the east section of the outer Lingdingyang (S4), with areas of 477, 977, 503, and 549  $\text{km}^2$ , respectively (Fig. 4). The PAH sink flux of each subregion was estimated for 2011 to be 3363.56, 2978.96, 1648.92 and 1708.55  $\text{kg yr}^{-1}$ , respectively, and the total PAH sink flux in the PRE was 9699.98  $\text{kg yr}^{-1}$ . In 2019, the sink flux of each subregion was 1416.65, 1464.12, 654.81, and 1126.72  $\text{kg yr}^{-1}$ , respectively, and the total PAH sink flux of 2019 was 4662.31  $\text{kg yr}^{-1}$ . S1 and S2 represented the inner Lingdingyang region, and S3 and S4 represented the outer Lingdingyang region. The sink flux of inner Lingdingyang region were

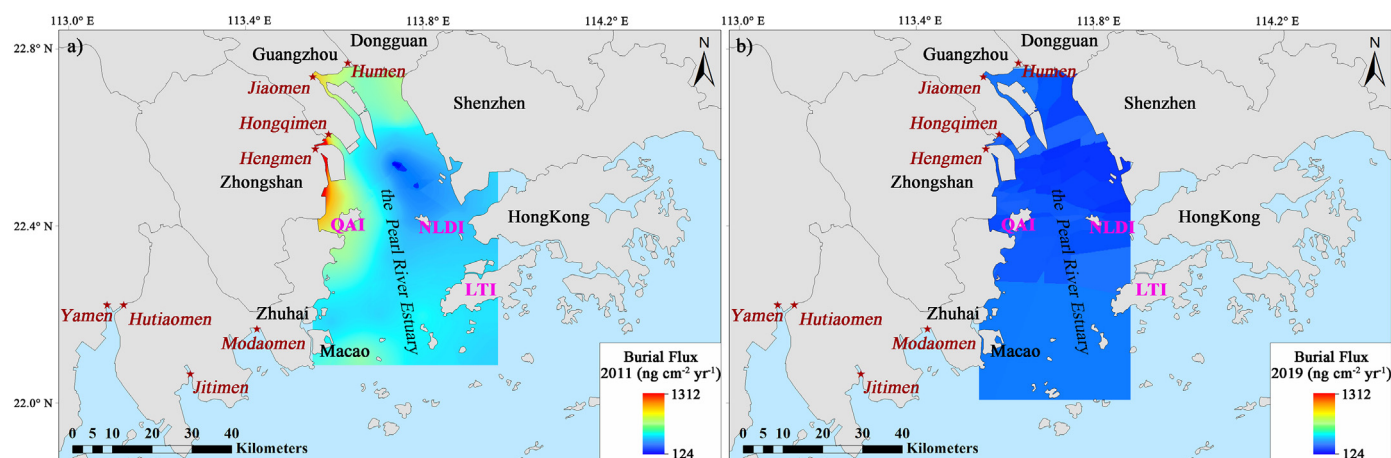


Fig. 5. Distribution pattern of PAHs deposition fluxes in 2011 (a) and 2019 (b).

6342.52 kg yr<sup>-1</sup> for 2011 and 2880.77 kg yr<sup>-1</sup> for 2019, while those of outer Lingdingyang region is 3357.47 kg yr<sup>-1</sup> for 2011 and 1781.53 kg yr<sup>-1</sup> for 2019. To conclude, the PRE presented obvious PAHs retention effect by surface sediment, the burial efficiency of the inner Lingdingyang region were about 2 times higher than outer Lingdingyang region in both 2011 and 2019.

Annual deposition fluxes of PAHs were evaluated in regional scale to compare the burial capacity of different regions (Table S6). In agreement with the mass inventories, the PAHs deposition flux of the PRE has been decreasing from 2002 to 2019. Burial capacity of the PRE was lower than Changjiang Subaqueous Delta mud area (SCDMA), East China Sea and the Gulf of Lion, but higher than Gulf of Mexico, Gulf of Thailand and Beibu Gulf. Therefore, sediments of the PRE have served as an important reservoir of PAHs from the PRD and a potential PAHs source to the global oceans.

### 3.4. Controlling factors on the fate of PAHs

#### 3.4.1. Anthropogenic impacts

Since PAHs are mainly originated from incomplete combustion of organic matters and fossil fuels, their compositions are well correlated with anthropogenic activities. Therefore, PAHs are also useful geochemical markers for anthropogenic impact. The variations in the PAH concentration, composition and source in the PRE indicated that the type and composition of energy sources have changed from 2011 to 2019. To further figure out the reasons, we analyzed change of the total consumption and composition of energy sources in Guangdong Province during 2010–2020 (Fig. 6).

Though the total consumption of energy sources has largely increased from  $2.2 \times 10^8$  tons of Standard Coal Energy (SCE) in 2010 to  $3.3 \times 10^8$  tons of SCE in 2020, the total percentage of coal and crude oil in consumed energy sources has declined from 74.2% in 2010 to 58.5% in 2020 and the total percentage of natural gas, primary electricity and other energy has increased from 25.8% in 2010 to 41.6% in 2020. Obviously, the structure of the consumption of energy sources in the PRD has been upgraded from unsustainable energy from fossil fuel combustion to renewable and clean energy types, as projected in the Comprehensive Improvement of Water Environment in the Pearl River and the South Guangdong Water Purification Action Plan (2013–2020), which has been implemented by the Guangdong Province government during the past decade.

PAH composition and qualitative analysis of MDR showed that the dominant PAH source in the PRE has shifted from petroleum pollution to petroleum combustion over the past years, which is consistent with the transformation of energy structure and implementation of pollution control policy in the GBA. A previous study reported that in the sediment core,

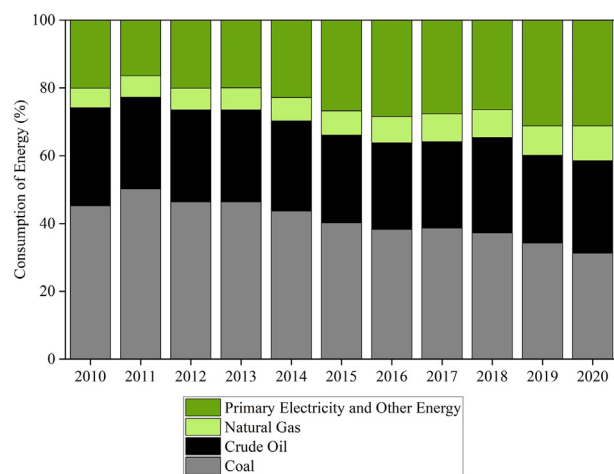


Fig. 6. Composition of the consumption of energy sources in the Guangdong Province during 2010–2020. Data were obtained from the Guangdong Statistical Yearbook (2021).

PAHs originated from vehicles sharply increased since 2000. However, no similar increasing trends were found in other PAHs (Cai et al., 2017). Similarly, vehicular exhaust related PAHs were also reported to increase in many developing countries (Zhang et al., 2013), where increasing urbanization has resulted in decentralized workplaces and higher dependence on vehicles (Van Metre et al., 2000). As a result of the transformation of energy structure and implementation of pollution control policy in the GBA, the total PAH concentration in the PRE has decreased by 50% over the past years.

#### 3.4.2. Influence of sedimentary environment

In order to figure out the influence of sedimentary environment on the PAHs in the PRE, the grain size (% sand, % silt, and % clay) and TOC content (%) were measured for surface sediments collected in 2019 (Fig. S3). Grain size analysis indicated that the major component in the PRE was silt (63.33%), followed by clay (30.63%) and sand (6.04%). Clay and silt were also the dominant sediment types of the surficial sediment collected in 2007, but the average component was 49% and 46%, respectively (Zhang et al., 2013). In 2019, the clay content in the surficial sediment ranged from 8% to 38%, which was substantially lower than in 2007 (30–50%). Therefore, the grain size values of this study showed a coarsening trend after 2007, which might be a result of the decline of the riverine inputs sediment in the past 30 years (Zhao et al., 2017). The reduction of the riverine sediments mostly affected by human perturbations such as deforestation and dam construction which corresponded to Economic Reform and Open Up in China (Li et al., 2022).

Compared to 2011 (0.09%–2.95%,  $1.13\% \pm 0.49\%$ ), TOC content of the surficial sediments was also lower in 2019 (0.09%–1.04%,  $0.61\% \pm 0.28\%$ , Fig. S3a, b). This decreasing trend of TOC in the PRE was also reported in sediment core in the past decade. And the reduction of TOC content was attributed to human perturbations such as deforestation and dam construction (Li et al., 2022). In 2019, the TOC content was high in the middle part of the estuary and low in the head of the estuary (Fig. S3b), and the high TOC contents in the southern part of QAI and middle part of QAI and NLDI can be linked to the local high levels of fine sediment (Fig. S3c). In addition, fine sediment was also found at the head estuary. Coarse sand was mainly observed near Shenzhen Bay where TOC contents were low (Fig. S3). Silt was mainly observed at the southern part of the estuary.

The relationships between concentrations of total PAHs and TOC contents or grain size of sediment in the western and eastern sections of the PRE were further analyzed to explore the influences of these factors on the PAH distribution (Tables S7 and S8). The sediment deposition rate in the West Shoal is higher than in the Middle and East Shoal (Fig. 4), and thus the PRE was divided into two sections (western and eastern) for further discussion. In the western section of the PRE, the TOC content showed a strong negative correlation relationship with the sand content ( $r = -0.777, p < 0.01, n = 12$ ), and significant positive correlation relationships with both the silt ( $r = 0.717, p < 0.01, n = 12$ ) and clay contents ( $r = 0.787, p < 0.01, n = 12$ ). The correlation analysis results demonstrated that PAH distribution in the western section of the PRE was consistent with the finer silt, clay, and TOC content, which is in good agreement with the results reported by Hao et al. (2021) in the Eastern China Marginal Seas. However, in the eastern section of the PRE, opposite correlations were found between  $\Sigma_{16}$  PAH concentrations and sand, silt, and clay contents (Table S8), which can be attributed to the difference in the sedimentary regimes between these two sections. Besides, the sedimentary environment in the eastern section of the PRE is disturbed by more intensive human activities, such as channel dredging and sand mining, which lead to the heterogeneous nature of sediments in the eastern section (Wei et al., 2021), thus further influencing the PAH distribution in the surface sediment.

The trapped sediment in the PRE has become more and more coarsening in recent decades, which implies a change in sedimentary environment of the estuary. The coarsening trend was in consistent with the decline in the TOC content in 2011 and 2019, for TOC easily absorbed on fine particles. The variation in sedimentary properties and environment caused by human perturbations strongly influenced the distribution and burial of



sediment-associated materials such as PAHs and organic carbon (Wang et al., 2022).

#### 4. Conclusions

A comprehensive investigation on PAHs distribution, source variation, mass inventories and deposition flux were conducted in 2011 and 2019, respectively, to elucidate the controlling factors on PAHs in the PRE.

We found the average concentration of  $\Sigma_{16}$  PAHs has decreased by 50% compared to 2011, and the dominant components changed from LMW PAHs to HMW PAHs. The high PAH concentrations was linked with anthropogenic impacts; The dominant PAHs source have shifted from petroleum to traffic emission, which indicated that the transformation of the energy structure and the effectiveness of regulation of reducing PAH inputs in the past years; The averaged PAHs deposition fluxes of 2019 in the PRE was  $215.52 \pm 246.63 \text{ ng cm}^{-2} \text{ yr}^{-1}$ , and about  $203.39 \text{ ng cm}^{-2} \text{ yr}^{-1}$  lower than 2011. Moreover, the PRE sediment presented prominent PAHs retention effect, and the burial efficiency of the inner Lingdingyang region were about 2 times higher than outer Lingdingyang region in both surveys.

The variation in sedimentary properties and environment inevitably influenced the distribution and burial fate of sediment-associated PAHs. Although the foreseen rapid economic development in the GBA together with the global climate change might enhance PAHs concentration, the anticipated countermeasures against environmental pollution complicate the problem and it remains unclear how the PAHs in the PRE will change in future, which calls for a continuous monitoring.

#### CRediT authorship contribution statement

Yali Li: Conceptualization, Writing-Original draft preparation and reviewing and editing, Funding acquisition.

Nairong Guo, Ke Yuan, Baowei Chen and Maofeng Hua: Investigation, Visualization, Formal analysis.

Junjie Wang: Writing-Review & Editing, Funding acquisition.

Ying Yang: Investigation, Supervision, Writing-Review & Editing, Funding acquisition.

Jing Yu, Jingyan Hu and Run Lu: Investigation.

Shichun Zou: Conceptualization, Supervision, Writing-Review & Editing.

#### Data availability

Data will be made available on request.

#### Declaration of competing interest

The authors declare that they have no known competing financial interests or personal relationships that could have appeared to influence the work reported in this paper.

#### Acknowledgements

This study was supported by the Guangdong Basic and Applied Basic Research Foundation (NO.2019A1515110248), National Natural Science Foundation of China (NO. 42175118), Key-Area Research and Development Program of Guangdong Province (NO. 2020B1111020002), 2019 Guangzhou Innovation and Entrepreneurship Leader Team (NO. 201909010008) and funding from the Dutch Ministry of Education, Culture and Science through the Netherlands Earth System Science Center (NESSC) (J.W.). We acknowledged Dr. Heng Zhang, Dr. Lei Zhu and Dr. Xiao Ma of Sun Yat-sen University for their support in sedimentary regime analysis and proof reading. We were also grateful to Xiaomin Wang, Junxin Wang, Shuangni Wei of Sun Yat-sen University for their efforts in chemical analysis.

#### Appendix A. Supplementary data

Supplementary data to this article can be found online at <https://doi.org/10.1016/j.scitotenv.2022.160870>.

#### References

- Aiken, G.R., Gilmour, C.C., Krabbenhoft, D.P., Orem, W., 2011. Dissolved organic matter in the Florida everglades: implications for ecosystem restoration. *Crit. Rev. Environ. Sci. Technol.* 41, 217–248.
- An, Y., Hong, S., Yoon, S.J., Cha, J., Shin, K.H., Khim, J.S., 2020. Current contamination status of traditional and emerging persistent toxic substances in the sediments of Ulsan Bay, South Korea. *Mar. Pollut. Bull.* 160 (11560).
- Bouloubassi, I., Roussiez, V., Azzoug, M., Lorre, A., 2012. Sources, dispersal pathways and mass budget of sedimentary polycyclic aromatic hydrocarbons (PAH) in the NW Mediterranean margin, Gulf of Lions. *Mar. Chem.* 142, 18–28.
- Cai, M., Lin, Y., Chen, M., Yang, W., Du, H., Xu, Y., Cheng, S., Xu, F., Hong, J., Chen, M., Ke, H., 2017. Improved source apportionment of PAHs and Pb by integrating Pb stable isotopes and positive matrix factorization application (PAHs): a historical record case study from the northern South China Sea. *Sci. Total Environ.* 609, 577–586.
- Chen, S.J., Luo, X.J., Mai, B.X., Sheng, G.Y., Fu, J.M., Zeng, E.Y., 2006. Distribution and mass inventories of polycyclic aromatic hydrocarbons and organochlorine pesticides in sediments of the Pearl River Estuary and the northern South China Sea. *Environ. Sci. Technol.* 40, 709–714.
- Duan, L., Naidu, R., Thavamani, P., Meaklim, J., Megharaj, M., 2015. Managing long-term polycyclic aromatic hydrocarbon contaminated soils: a risk-based approach. *Environ. Sci. Pollut. Res.* 22, 8927–8941.
- Dudhagara, D.R., Rajpara, R.K., Bhatt, J.K., Gosai, H.B., Sachaniya, B.K., Dave, B.P., 2016. Distribution, sources and ecological risk assessment of PAHs in historically contaminated surface sediments at Bhavnagar coast, Gujarat, India. *Environ. Pollut.* 213 (338346).
- Fang, Y., Chen, Y.J., Tian, C.G., Lin, T., Hu, L.M., Huang, G.P., Tang, J.H., Li, J., Zhang, G., 2015. Flux and budget of BC in the continental shelf seas adjacent to Chinese high BC emission source regions. *Glob. Biogeochem. Cycle* 29, 957–972.
- Feng, S.S., Fan, F.L., 2018. Spatiotemporal changes of landscape pattern using impervious surface in Guangdong-Hong Kong-Macao Greater Bay Area, China. *Chin. J. Appl. Ecol.* 29, 2907–2914.
- Gu, Y.G., Lin, Q., Lu, T.T., Ke, C.L., Sun, R.X., Du, F.Y., 2013. Levels, composition profiles and sources of polycyclic aromatic hydrocarbons in surface sediments from Nan'ao Island, a representative mariculture base in South China. *Mar. Pollut. Bull.* 75, 310–316.
- Guangdong Provincial Bureau of Statistics, 2021. Guangdong Statistical Yearbook. [http://stats.gd.gov.cn/gdtjnj/content/post\\_3557537.html](http://stats.gd.gov.cn/gdtjnj/content/post_3557537.html).
- Han, B., Li, Q., Liu, A., Gong, J., Zheng, L., 2021. Polycyclic aromatic hydrocarbon (PAH) distribution in surface sediments from Yazhou Bay of Sanya, South China, and their source and risk assessment. *Mar. Pollut. Bull.* 162 (11800).
- Hao, Z., Xu, H., Feng, Z., Zhang, C., Zhou, X., Wang, Z., Zheng, J., Zou, X., 2021. Spatial distribution, deposition flux, and environmental impact of typical persistent organic pollutants in surficial sediments in the Eastern China Marginal Seas (ECMSs). *J. Hazard. Mater.* 407 (124343) 2021.
- Hu, J., Li, S., Geng, B., 2011. Modeling the mass flux budgets of water and suspended sediments for the river network and estuary in the Pearl River Delta, China. *J. Mar. Syst.* 88, 252–266.
- Huang, F.J., Lin, X.B., Hu, W.F., Zeng, F., He, L., Yin, K.D., 2021. Nitrogen Cycling Processes in Sediments of the Pearl River Estuary: Spatial Variations, Controlling Factors, and Environmental Implications. 206, No. 105545.
- Huang, K., Li, R., Yang, P.P., Pan, L.D., Zhang, L.Q., 2021. Distribution characteristics of soil total organic carbon in typical karst area and its response to different planting and management modes of slope farmland. *Sci. Soil Water Conserv.* 19, 37–46.
- Jia, T., Guo, W., Liu, W., Xing, Y., Lei, R., Wu, X., Sun, S., 2021. Spatial distribution of polycyclic aromatic hydrocarbons in the water-sediment system near chemical industry parks in the Yangtze River Delta, China. *Sci. Total Environ.* 754 (142176).
- Kanwischer, M., Bunke, D., Leipe, T., Moros, M., Schulz-Bull, D.E., 2020. Polycyclic aromatic hydrocarbons in the Baltic Sea - pre-industrial and industrial developments as well as current status. *Mar. Pollut. Bull.* 160 (111526).
- Lemieux, P.M., Lutes, C.C., Santoanni, D.A., 2004. Emissions of organic air toxics from open burning: a comprehensive review. *Prog. Energy Combust. Sci.* 30, 1–32.
- Li, B., Feng, C., Li, X., Chen, Y., Niu, J., Shen, Z., 2012. Spatial distribution and source apportionment of PAHs in surficial sediments of the Yangtze Estuary, China. *Mar. Pollut. Bull.* 64, 636–643.
- Li, Y., Guo, N., Zou, X., Li, P., Zou, S., Luo, J., Yang, Y., 2021. Pollution level and health risk assessment of polycyclic aromatic hydrocarbons in marine fish from two coastal regions, the South China Sea. *Mar. Pollut. Bull.* 168 (112376).
- Li, Y., Zou, X., Zou, S., Li, P., Yang, Y., Wang, J., 2021b. Pollution status and trophic transfer of polycyclic aromatic hydrocarbons in coral reef ecosystems of the South China Sea. *ICES J. Mar. Sci.* 78, 2053–2064.
- Li, W., Li, X., Zhao, X., Sun, C., Nie, T., Hu, Y., Wang, C., 2022. Impacts of climate change and human perturbations on organic carbon burial in the Pearl River Estuary over the last century. *Front. Mar. Sci.* 9 (848757).
- Lin, G.M., Lin, X.B., 2022. Bait input altered microbial community structure and increased greenhouse gases production in coastal wetland sediment. *Water Res.* 218 (118520).
- Lin, T., Hu, L., Guo, Z., Zhang, G., Yang, Z., 2013. Deposition fluxes and fate of polycyclic aromatic hydrocarbons in the Yangtze River estuarine-inner shelf in the East China Sea. *Glob. Biogeochem. Cycle* 27, 77–87.
- Lin, S.L., Tsai, J.H., Chen, S.J., Huang, K.L., Lin, C.C., Huang, H.T., Hsieh, Y.C., Chiu, C.H., 2017. Emissions of polycyclic aromatic hydrocarbons and particle-bound metals from a

- diesel engine generator fueled with waste cooking oil-based biodiesel blends. *Aerosol Air Qual. Res.* 17, 1679–1689.
- Lin, F., Han, B., Ding, Y., Li, Q., Gao, W., Zheng, L., 2018. Distribution characteristics, sources, and ecological risk assessment of polycyclic aromatic hydrocarbons in sediments from the Qinhuangdao coastal wetland, China. *Mar. Pollut. Bull.* 127, 788–793.
- Liu, L.Y., Wang, J.Z., Wei, G.L., Guan, Y.F., Zeng, E.Y., 2012. Polycyclic aromatic hydrocarbons (PAHs) in continental shelf sediment of China: implications for anthropogenic influences on coastal marine environment. *Environ. Pollut.* 167, 155–162.
- Maria, C.B., Dario, M., Paolo, P., 2018. PMF5.0 vs. CMB8.2: an inter-comparison study based on the new European SPECIEUROPE database. *Atmos. Res.* 201, 181–188.
- Nedwell, D.B., Jickells, T.D., Trimmer, M., Sanders, R., 1999. Nutrients in estuaries. *Adv. Ecol. Res.* 29, 43–92.
- Neff, J.M., 1979. Polycyclic Aromatic Hydrocarbons in the Aquatic Environment: Sources: Sources, Fates and Biological Effects. Applied Science Publishers, Michigan.
- Oliva, A.L., Quintas, P.Y., Ronda, A.C., Marcovecchio, J.E., Arias, A.H., 2020. First evidence of polycyclic aromatic hydrocarbons in sediments from a marine protected area within Argentinean Continental Shelf. *Mar. Pollut. Bull.* 158 (111385).
- Onozato, M., Nishigaki, A., Okoshi, K., 2020. Impact of the great East Japan earthquake on polycyclic aromatic hydrocarbons in sediments on the coast of Matsushima Bay, Northern Japan. *Polycycl. Aromat. Compd.* 40, 1291–1301.
- Paatero, P., Tapper, U., 1994. Positive matrix factorization: a non-negative factor model with optimal utilization of error estimates of data values. *Environmetrics* 5.
- Pintado-Herrera, M.G., Wang, C., Lu, J., Chang, Y.P., Chen, W., Li, X., Lara-Martin, P.A., 2017. Distribution, mass inventories, and ecological risk assessment of legacy and emerging contaminants in sediments from the Pearl River Estuary in China. *J. Hazard. Mater.* 323, 128–138.
- Qin, Y., Zheng, B., Lei, K., Lin, T., Hu, L., Guo, Z., 2011. Distribution and mass inventory of polycyclic aromatic hydrocarbons in the sediments of the south Bohai Sea, China. *Mar. Pollut. Bull.* 62, 371–376.
- Ribeiro, A.M., Martins da Rocha, C.C., Jaegger Franco, C.F., Fontana, L.F., Pereira Netto, A.D., 2012. Seasonal variation of polycyclic aromatic hydrocarbons concentrations in urban streams at Niterói City, RJ, Brazil. *Mar. Pollut. Bull.* 64, 2834–2838.
- Strong, D.J., Flecker, R., Valdes, P.J., Wilkinson, I.P., Rees, J.G., Zong, Y.Q., Lloyd, J.M., Garrett, E., Pancost, R.D., 2012. Organic matter distribution in the modern sediments of the Pearl River Estuary. *Org. Geochem.* 49, 68–82.
- USEPA (United States Environmental Protection Agency), 1992. The United States Experience With Economic Incentives to Control Environmental Pollution.
- Van Metre, P.C., Mahler, B.J., Furlong, E.T., 2000. Urban sprawl leaves its PAH signature. *Environ. Sci. Technol.* 34, 4064–4070.
- Vila-Costa, M., Cerro-Galvez, E., Martinez-Varela, A., Casas, G., Dachs, J., 2020. Anthropogenic dissolved organic carbon and marine microbiomes. *ISME J.* 14, 2646–2648.
- Wang, Z., Zheng, Y., Zhao, B., Zhang, Y., Liu, Z., Xu, J., Chen, Y., Yang, Z., Wang, F., Wang, H., He, J., Zhang, R., Abliz, Z., 2015. Human metabolic responses to chronic environmental polycyclic aromatic hydrocarbon exposure by a metabolomic approach. *J. Proteome Res.* 14, 2583–2593.
- Wang, C., Zou, X., Gao, J., Zhao, Y., Yu, W., Li, Y., Song, Q., 2016. Pollution status of polycyclic aromatic hydrocarbons in surface sediments from the Yangtze River Estuary and its adjacent coastal zone. *Chemosphere* 162, 80–90.
- Wang, C.L., Zou, X.Q., Zhao, Y.F., Li, Y.L., Song, Q.C., Wang, T., Yu, W.W., 2017. Distribution pattern and mass budget of sedimentary polycyclic aromatic hydrocarbons in shelf areas of the Eastern China Marginal Seas. *J. Geophys. Res.-Oceans* 122, 4990–5004.
- Wang, P., Mi, W., Xie, Z., Tang, J., Apel, C., Joers, H., Ebinghaus, R., Zhang, Q., 2020. Overall comparison and source identification of PAHs in the sediments of European Baltic and North Seas, Chinese Bohai and Yellow Seas. *Sci. Total Environ.* 737 (139535).
- Wang, L., Du, W., Yun, X., Chen, Y., Zhu, X., Shen, H., Shen, G., Liu, J., Wang, X., Tao, S., 2022. On-site measured emission factors of polycyclic aromatic hydrocarbons for different types of marine vessels. *Environ. Pollut.* 297 (118782).
- Wei, X., Cai, S.Q., Zhan, W.K., Li, Y.N., 2021. Changes in the distribution of surface sediment in Pearl River Estuary, 1975–2017, largely due to human activity. *Cont. Shelf Res.* 228 (104538).
- Xiang, N., Jiang, C., Yang, T., Li, P., Wang, H., Xie, Y., Li, S., Zhou, H., Diao, X., 2018. Occurrence and distribution of polycyclic aromatic hydrocarbons (PAHs) in seawater, sediments and corals from Hainan Island, China. *Ecotoxicol. Environ. Saf.* 152, 8–15.
- Yang, B., Zhou, L., Xue, N., Li, F., Li, Y., Vogt, R.D., Cong, X., Yan, Y., Liu, B., 2013. Source apportionment of polycyclic aromatic hydrocarbons in soils of Huanghuai Plain, China: comparison of three receptor models. *Sci. Total Environ.* 443, 31–39.
- Yang, C., Li, Q., Zhao, T., Liu, H., Gao, W., Shi, T., Guan, M., Wu, G., 2019. Detecting spatio-temporal features and rationalities of urban expansions within the Guangdong-Hong Kong-Macau Greater Bay Area of China from 1987 to 2017 using time-series Landsat images and socioeconomic data. *Remote Sens.* 11 (2215).
- Yuan, K., Wang, X., Lin, L., Zou, S., Li, Y., Yang, Q., Luan, T., 2015. Characterizing the parent and alkyl polycyclic aromatic hydrocarbons in the Pearl River Estuary, Daya Bay and northern South China Sea: influence of riverine input. *Environ. Pollut.* 199, 66–72.
- Yunker, M.B., Backus, S.M., Graf Pannatier, E., Jeffries, D.S., Macdonald, R.W., 2002. Sources and significance of alkane and PAH hydrocarbons in Canadian Arctic Rivers. *Estuar. Coast. Shelf Sci.* 55, 1–31.
- Zhang, S.C., Huang, H.P., 2005. Geochemistry of palaeozoic marine petroleum from the Tarim Basin, NW China: part 1. Oil family classification. *Org. Geochem.* 36, 1204–1214.
- Zhang, Y., Wang, X., Barletta, B., Simpson, I.J., Blake, D.R., Fu, X., Zhang, Z., He, Q., Liu, T., Zhao, X., Ding, X., 2013. Source attributions of hazardous aromatic hydrocarbons in urban, suburban and rural areas in the Pearl River Delta (PRD) region. *J. Hazard. Mater.* 250–251, 403–411.
- Zhang, G., Cheng, W., Chen, L., Zhang, H., Gong, W., 2019. Transport of riverine sediment from different outlets in the Pearl River Estuary during the wet season. *Mar. Geol.* 415 (105957).
- Zhang, R., Li, T., Russell, J., Zhang, F., Xiao, X., Cheng, Y., Liu, Z., Guan, M., Han, Q., 2020. Source apportionment of polycyclic aromatic hydrocarbons in continental shelf of the East China Sea with dual compound-specific isotopes ( $\delta^{13}C$  and  $\delta^2H$ ). *Sci. Total Environ.* 704 (135459).
- Zhao, M., Wang, W., Liu, Y., Dong, L., Jiao, L., Hu, L., Fan, D., 2016. Distribution and sources of polycyclic aromatic hydrocarbons in surface sediments from the Bering Sea and western Arctic Ocean. *Mar. Pollut. Bull.* 104, 379–385.
- Zhao, H., Wang, X., Li, X., 2017. Quantifying grain-size variability of metal pollutants in road-deposited sediments using the coefficient of variation. *Int. J. Environ. Res. Public Health* 14 (850).
- Zhao, X., Jin, H., Ji, Z., Li, D., Kaw, H.Y., Chen, J., Xie, Z., Zhang, T., 2020. PAES and PAHs in the surface sediments of the East China Sea: occurrence, distribution and influence factors. *Sci. Total Environ.* 703 (134763).
- Zhu, C.S., Li, L.J., Huang, H., Dai, W.T., Lei, Y.L., Qu, Y., Huang, R.J., Wang, Q.Y., Shen, Z.X., Cao, J.J., 2020. N-alkanes and PAHs in the southeastern Tibetan Plateau: characteristics and correlations with brown carbon light absorption. *J. Geophys. Res.-Atmos.* 125 (e2020JD032666).
- Zhu, L., Zhang, H., Guo, L., Huang, W., Gong, W., 2021. Estimation of riverine sediment fate and transport timescales in a wide estuary with multiple sources. *J. Mar. Syst.* 214 (103488).